6th International Conference on Contemporary Problems of Thermal Engineering
CPOTE 2020, 21-24 September 2020, Poland

On design and analysis of flow characteristics of the last stage of gas-steam turbine

Stanisław Głuch[1], Paweł Ziółkowski[1], Łukasz Witanowski[2], Michał Stajnke[2], Piotr Józef Ziółkowski[2], Janusz Badur[2]
[1]Gdańsk University of technology, Mechanical Faculty
e-mail:stanislaw.gluch@pg.edu.pl
e-mail: pawel.ziolkowski1@pg.edu.pl

[2]Institute of Fluid-Flow Machinery Polish Academy of Sciences

Keywords: Axial turbine, Blade design, Computational fluid dynamics, Last stage of low-pressure turbine , Twisted blade

Abstract

Research regarding blade design and analysis of flow have been conducted for over a century. Meanwhile new concepts and design approaches were created and improved. Advancements in information technologies allowed to introduce computational fluid dynamics (CFD) and computational flow mechanics (CFM). Currently a combination of mentioned methods is used for design of turbine blades. These methods enabled us to improve flow efficiency and strength of turbine blades. This paper relates to a new type turbine which is in the phase of theoretical analysis, because the working fluid is a mixture of steam and gas generated in wet combustion chamber. Conception of this cycle and thermodynamic calculations are presented in previous papers, therefore the main aim of this article is design and analysis of flow characteristics of the last stage of gas-steam turbine.

When creating the spatial model, the atlas of profiles of reaction turbine steps was used. In this paper results of CFD calculations of twisting of the last stage are presented. Blades geometry and the computational mesh are also presented. Triangles of velocity for selected dividing sections are presented. It is worth noting that the velocity along the pitch diameter varies greatly. Near the root it shows an action triangle, on the other hand, near the tip it presents a reaction type of triangle. Velocity fields and pressure fields show the flow characteristics of the last stage of gas-steam turbine. The net efficiency of the cycle is estimated as 54.35% regarding to enthalpy drop, however, the net efficiency taking into account the mechanical power determined from the stage theory is equal 52.61%.

1 Introduction

The work on turbine blade shaping dates back to the beginning of the last century [1], however, over the years new concepts have appeared [2,3]. Apart from the concepts themselves, a research tool was also developed which, starting from analytical tools [1], with the previous years transformed into analyses including sophisticated numerical tools [4,5]. At present, turbine companies are already based on a fully three-dimensional approach, both for solid-state stress analyses and for efficiency-enhancing flow analyses [6]. This paper refers to a turbine which is in the purely theoretical analysis phase, as the working medium is the steam-gas produced in a wet combustion chamber. The concept of this circulation was developed in the dissertation of P. Ziółkowski [7].

In work [8] the numerical analysis of a four stage low pressure steam turbine was presented. The thermodynamic behavior of the wet steam was reproduced by adopting a real gas model. Geometrical features and flow-path details consistent with the actual turbine geometry were included in the analysis using simple models. simple one-dimensional model of shrouded cavity was implemented, and its inclusion in the primary flow solver was described in detail. All these models were applied in the computation of the steam turbine, and computed spanwise distributions were compared to experimental ones at inlet/exit of the last stage. The models discussed in this paper were thought to be used as industrial tools suitable for turbomachinery design. They are aimed at capturing the relevant physics of some aspects which are usually neglected within the design process.

Paper [9] describes the features and analyzes the results of a zero dimensional model for the design of high efficiency small size ORC expanders. Starting from a previously developed 0D design tool for radial ORC expanders [10] able to account for the specific loss correlations across the rotor, a 3D design procedure for very small expanders was developed with the purpose of achieving an improved design, mainly concerning the geometry of the flow channel and the number of blades. The 3D geometry of the rotor was imported in commercial CFD packages. The improved design corresponds to the final fluid dynamics design of the rotor, with the improved blade geometry and a more suitable number of blades. The results of the 0D and 3D models applied to the reference case showed a satisfactory agreement, confirming the reliability of the 0D design tool as the basis for the definition of the overall geometry and working parameters of the machine.

Authors of [11] shape optimization of a 3D nozzle and a 2D turbine blade cascade was presented based on CFD simulation of turbulent nucleating transonic wet steam flow in the corresponding flow passage. Both the liquid and gaseous phases were treated as continua and for each phase the conservation laws were solved together with proper source terms modeling the mass transfer and momentum exchange between two phases. A nonequilibrium condensation model based on classical nucleation and growth theory was utilized as well. Main conclusion of this work is that in analyzed cases k-ω SST turbulence model more accurately predicts the wet steam flow field in comparison to the well-known k-ε model for Moore's ''Nozzle A" and Dykas's turbine blade cascade.

In paper [12] Large-scale aerodynamic and structural interaction analysis was introduced to analyze steam turbine last stage blade. The two different kind of the unsteady flow analyses were carried out. The results shows that the nozzle blade shock wave reflections on the rotor blade surface seems to be one of main origin that induce the flow unsteadiness and blade vibration in operating condition. The unsteady flow analysis of low load flow condition was carried out. This result shows the important flow features in the last stage. Robust data interpolation software was developed and proved to be able to use in the present system. Existing measured data of the model steam turbine and the wheel box test facility was used to assume damping factors and to validate the unsteady flow analysis and CSD (Computational Solid Dynamics) result.

The recent technologies on developments and designs of last-stage long blades for steam turbines are explained in [13]. Technical features of last-stage long blades are high centrifugal force, high blade speed, 3D flow, wet steam flow, and relatively large unsteady flow forces during low-load operations. Regarding future trends in last-stage long-blade technologies, recent studies cited in this chapter indicate that the accuracy of unsteady flow forces and blade vibration stresses in very low load conditions is being enhanced by employing state-of the-art CFD, CSD, and (FSI) Fluid Solid Interaction analysis. These new technologies, together with modern material science and fracture analysis based on strength

of material science, will provide some breakthroughs to further increase annulus areas. The redesign of existing blades for enhancement of low-load operation ranges employing these new technologies may bring more opportunities for steam turbine power plants because these power plants need to be operated to control electrical grid fluctuations due to the increase in the numbers of renewable-energy power plants.

Authors of [14] performed numerical study aimed at investigating the steady and unsteady interactions between the components of a two-stage axial turbine. They found out that the expansion rate and flow range are mainly controlled by the first stage. First stage wakes, secondary flows and vortices cause flow perturbations and losses to the second which persist downstream. Since the flow field is very affected by the wakes and vortices, a better design has to account for the optimum clocking position. In order to reduce the pressure loss due to the first stage tip leakage and vortices, a better flow control should be managed in the first rotor and second NGV and consider the effects of the gap between blade-rows.

Numerical studies have been conducted in [15] to understand the rotating instability previously experimentally identified at low mass flow rates in a model steam turbine stage. An initial CFD analysis using a time-domain RANS solver is able to capture a large scale separated flow pattern, which is compared well with the experimentally observed one. The 3D vertical flow pattern observed in the experiment is reproduced in the 3D calculation. The results consistently show that a rotating pattern non synchronized with the rotor speed exists at low mass flow conditions. The dominant frequency for the tip section identified by the Fourier transform is a higher (by 50%) than the experimental value and shifts when the mass flow rate is changed. The results suggest that the rotating speed of the patterns as seen in the stationary frame of reference is about a half of the rotor rotation speed. On the other hand, the near hub section is much more stable with no clearly identifiable rotating patterns found at low mass flow conditions.

The aim of the work is to adopt the free vortex law to the gas- steam turbine, and further to analyze the nature of the flow using CFD tools. Use of gas-steam as working fluid is a new concept. Analyze of results would allow to preliminary determine possible challenges in construction of this kind of turbine and recognize differences between analyzed stage and conventional steam turbine stage.

2 The case under consideration

This gas-steam turbine consists of high-pressure and low-pressure part (Fig 1). Fig.1 shows a diagram of a compact gas-steam power plant, where the key element is the original "wet combustion chamber" (WCC), which is a steam-gas generator. In this chamber (WCC), the product of the aerobic combustion of gases, combined with the "nano production" of steam, is a working medium containing about 80-90% steam and 20-10% CO_2. The exact data are shown in Table 1. It is therefore important to separate water vapour from CO_2 accordingly. The original idea proposed in [7] is also: 1) introduction of a streamer as a spray/jet condenser that condenses water and separates CO_2 and 2) use of a gas-steam turbine. Fig. 2 presents the shape of the last expander stage to ensure optimal use of the working medium enthalpy in GT+GTin. The turbine consists of one high pressure housing and one low-pressure, two outlet housing.

Table 1: Parameters of mixture and computational domain used in CFD simulation of a last turbine stage

$t_0 = 336.794$	°C
$\omega = 3000.$	rpm
$p_2 = 0.07955$	bar
$p_0 = 0.16225$	bar
X_{CO2} X_{H2O} X_{N2}	Sum
0.0894 0.9084 0.0022	1
Y_{CO2} Y_{H2O} Y_{N2}	Sum
0.1933 0.8037 0.003	1

The number of stages of the high (27 stages) and low-pressure part (6 stages in both directions) of the turbine were determined, together with the kinematics and velocity vectors for subsequent stages of the axial turbine. The low-pressure part has two outlets. The length of the rotor blade of the last stage is 1587 mm (Fig.2). The design process takes into account the law of variation of the velocity peripheral component of the working medium along the radius of the turbine blade and it is conducted in a discrete way so that a 3D drawing of the resulting geometry can be performed. The circumferential velocity varies from 262 m/s near the blade hub to 771 m/s near the blade tip.

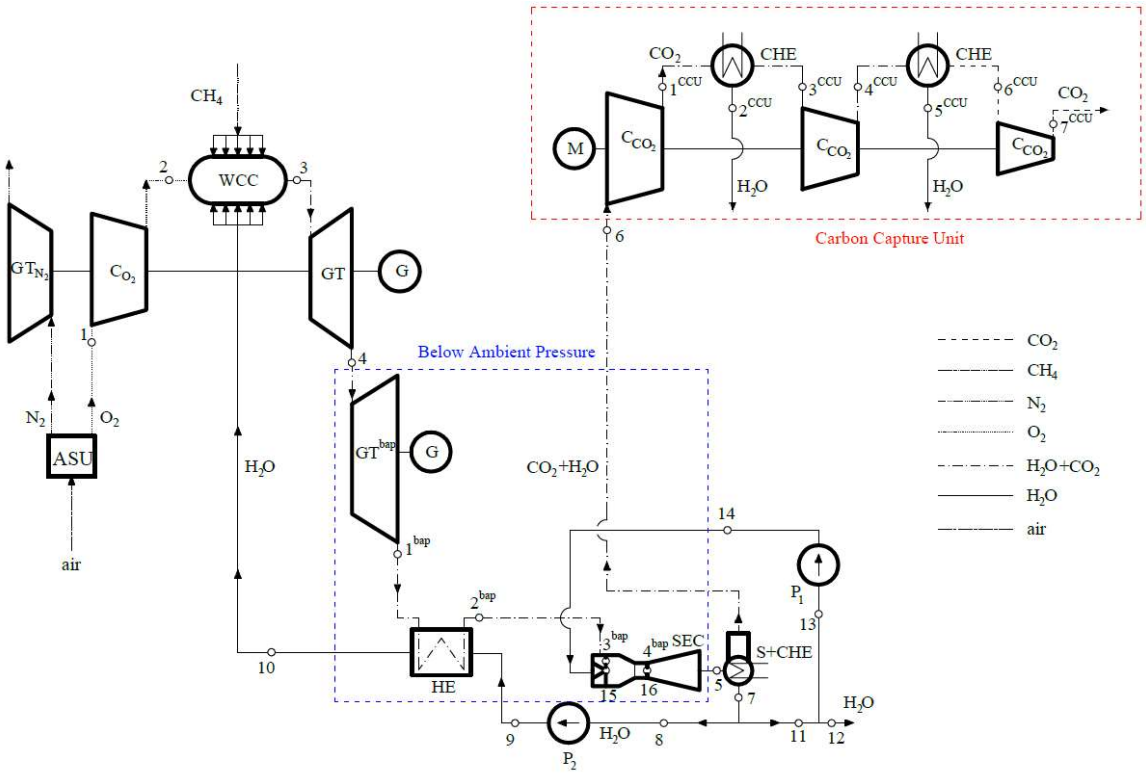

Figure 1: The double Brayton cycle with oxy-combustion and CO_2 capture (DBCOCC), where WCC – wet combustion chamber, GT+GT^{bat}– gas turbine divided into two parts, SEC – spray ejector condenser, ASU – air separation unit, C - compressor, HE – heat exchanger, CHE + S – condensate-cooler heat exchanger and separator, CHE – cooling heat exchanger, M – motor, G – generator, P_1 – supply water pump, P_2 –water pump for cooling combustion chamber, GT_{N2} – expander N_2, C_{CO2} –CO_2 compressor.

Fig. 2 shows a 3D geometry of the stator and rotor blade designed based on the free vortex law. The last stage of turbine is always a peculiar one, not only it is challenging from the material strength point of view, but also regarding fluid flow. Numerical analysis of this particular case also provides difficulties. To ensure that simulation will be performed correctly discretization of the analyzed domain must be done correctly with inclusion of crucial elements. For this purpose, hexahedral mesh has been chosen, as one that provides excellent accuracy and relatively low elements count. In this case to perform calculations in reasonable time period mesh consisting of 4 000 000 hexahedral elements was used. Mesh limits were set on the maximum face angle (165°), minimum face angle (15°), connectivity number (12), maximum and minimum volume ratio (10 and 0) and maximum edge length ratio (500).

Cross section through the domain was shown in the Fig. 3, on the left part the stator's blade mesh is portrayed and on the right side is mesh used on rotor blades. Mesh used in rotor stage was finer due to more complex phenomena's occurring compared to stator hence for better reproduction of real processes it is necessary. In this paper only one channel was modelled and in circumferential direction periodic boundary condition was implemented to imitate the impact of other turbine blades on the fluid flow without unnecessarily increasing elements count.

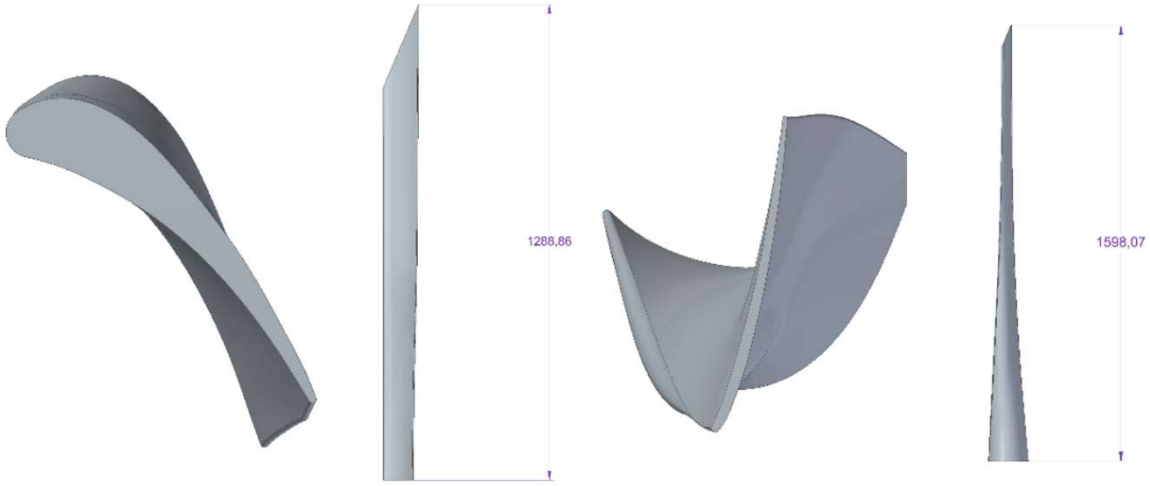

Figure 2: View from the top and front – respectively stator and rotor blade.

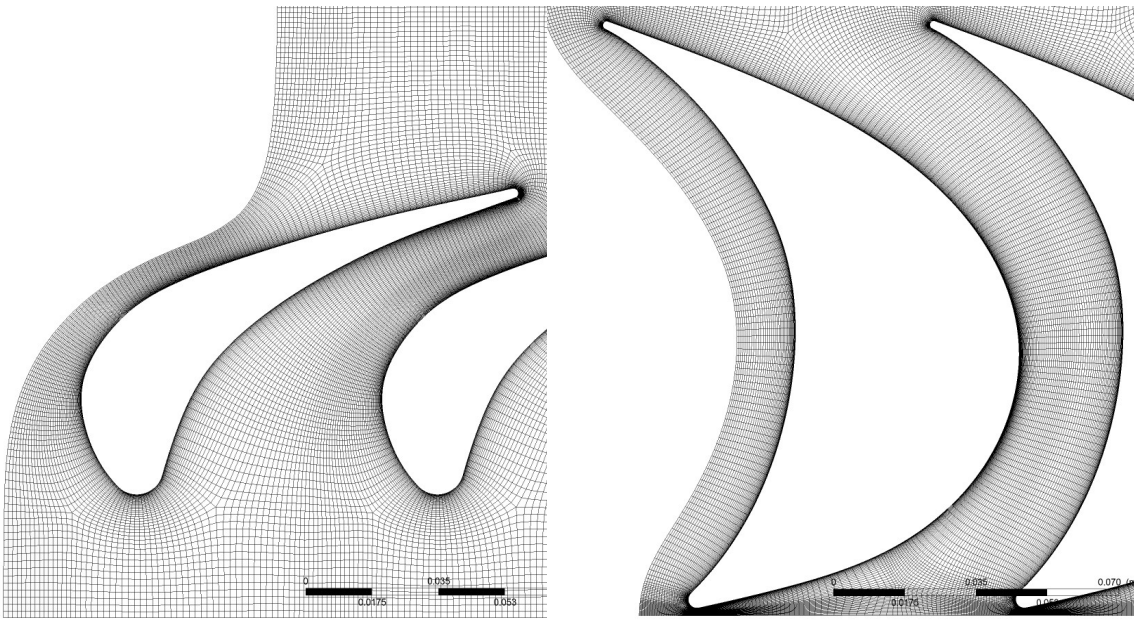

Figure 3: Mesh used in numerical simulation, respectively stator and rotor on the left and right side of the figure.

3 Mathematical model

The calculation is based on two steps, namely: 1) determination of the shape of the last stage based on the free vortex law; 2) calculation of the flow based on CFD tools.

3.1 Twisted blade model

The kinematics of the stage undergoes significant changes as we disregard the assumption that the channel high following the radius is homogeneous. In fact, the flow fields change with the radius. In order to increase the efficiency of the turbine, the shape of the blades must be adjusted to the changing flow. It is accomplished by changing the angles α and β in order to adjust the blade shape to the changing peripheral speed u. The twisting was performed using the free vortex method presented in Professor

Perycz's book [16], as this method has been described most precisely. However, in the further part of this work we will also refer to Professor Szewalski's proposal [1-3].

Usually, the law of coiling of the second blade, i.e. the law of variation of the peripheral component of the speed of the working fluid in radius direction, is rather suitable in a discrete form, and differently for the inlet to the vane channel and for the outlet. In engineering practice, it is assumed that the velocity component c_{2u} at the inlet is to be as low as possible and should not be increased unnecessarily due to the decrease in efficiency by dissipation of kinetic energy of the medium operating at the outlet [16]. Thus, the free vortex procedure is based on the slow vortex method, but the most important calculation steps will be introduced for clarity. Starting from the division of the blade height in a discrete way into 15 sections:

$$\Delta l_k = \frac{l_k}{n} \; ; \; \Delta l_w = \frac{l_w}{n} \tag{1}$$

It is equally important to determine the inflow angle α_1 in subsequent sections by using the relationship:

$$\tan \alpha_{1ust} = \frac{\alpha_{1m} \cdot \pi/180}{r_{ust}/r_m} \; ; \; \tan \alpha_1 = \frac{r_2}{r_{ust}} \cdot \tan \alpha_{1ust} \tag{2}$$

where: r_m - average radius, α_{1m}- average angle of inlet, α_{1ust} - angle of inlet at the foot, $r_2$radius of the rotor for a given section, r_{ust} - radius at the foot of the rotor. Reactivity of the step is determined based on the formula:

$$\rho = 1 - (1 - \rho_{ust}) \cdot (\frac{r_{ust}}{r_1})^k \tag{3}$$

where: ρ_{ust} = 0.1 is assumed as initial, r_1 - radius of the steering wheel in a given section of the discernment, $k = 2 \cos \alpha_1$ coefficient at the correction of reactivity. Based on the continuity equation we determine the stream of mass on particular sections:

$$\Delta \dot{m} = \frac{\mu_1 \cdot c_{1s} \cdot \Delta A_1 \cdot \sin \alpha_1}{v_{1s}} \tag{4}$$

where: $\Delta A_1 = 2 \cdot \pi \cdot r_2$ is the surface area of the given section, μ_1 is the coefficient, c_{1s} absolute speed, v_{1s} relative speed. The calculation procedure also determines the angle β and the speed components for the individual speed triangles, blade losses for subsequent sections, power and efficiency.

The calculation is carried out in an iterative manner and the parameter to be compared is the mass flow, as the value of the sum of $\Delta \dot{m}$ from the individual sections of the discernment shall correspond to $\dot{m} = 91.15$ kg/s.

The initial assumptions for a twisted stage are collected in Table 2. In turn, the assumed parameters of the step needed to carry out the calculation of the twisting for selected sections of the discretization are presented in Table 3. In the Table 4 results of the calculations for the five divisional sections were presented. Section number 8 is located on the pitch diameter. Due to very large changes in the value of peripheral velocity, u, there are large changes in reactivity, angles and velocity along the radius. The value of peripheral speed, u, varies from u =262 m/s to u =771 m/s. The sound velocity in this area of the pair fluctuates around 440 m/s.

It should be noted that near the hub the blade is impulse at the foot and extremely high reaction ratio at the apex. The minimum reaction ratio of 0.1 is at the hub. This value should not fall below ρ =0.1 so that there is no negative degree of reaction value during operation on partial power. Reaction ratio near the shroud is as high as ρ =0.89. Figure 4 shows the velocity triangles for selected divisional sections.

Table 2: Initial assumptions regarding twisted stage.

ρ_n	-	0.1
r_{n1}	m	0.820115209
r_{n2}	m	0.820115209
H_{sc}	kJ/kg	178.6120643
H_s	kJ/kg	165
l_k	m	1.293335645
l_w	m	1.578019487
ω	rad/s	314.1592654
α_1	°	22.5
p_0	MPa	0.016255325
h_0	kJ/kg	2695.346123
s_0	kJ/(kg·K)	8.254181075
$\dot{m}$	kg/s	91.15
c_0	m/s	164.9973594
n	-	15
Δl_k	m	0.086222376
Δl_w	m	0.105201299
α_{1n}	°	11.92069374

Table 3: Assumptions regarding chosen sections of a twisted blade.

parameter	unit	1	4	8	12	15
μ_1	-	0.94	0.94	0.94	0.94	0.94
μ_2	-	0.94	0.94	0.94	0.94	0.94
φ	-	0.935	0.95	0.95	0.95	0.95
ψ	-	0.925	0.935	0.935	0.935	0.935

Table 4: Results obtained in twisted stage

parameter	unit	1	4	8	12	15
r_1	m	0.8632	1.1218	1.4667	1.8116	2.0703
r_2	m	0.8727	1.1883	1.6091	2.03	2.3455
ρ	-	0.1906	0.5221	0.7152	0.8084	0.8503
u	m/s	274.17	373.32	505.52	637.72	736.87
α_1	°	14.661	19.008	24.95	30.089	33.623
c_{1s}	m/s	529.8	413.9	328.02	277.18	251.01
c_1	m/s	495.38	393.2	311.6	263.32	238.46
ΔA_1	m^2	0.4677	0.6078	0.7946	0.9814	1.1216
Δm	kg/s	2.471	3.896	5.807	7.57	8.85
β_2	°	20.988	19.127	16.476	13.861	12.262
l_u	kJ/kg	146.15	150.15	144.25	135.38	126.99
l_s	kJ/kg	158.04	156.09	154.27	153.28	152.75
η_u	-	0.9247	0.9619	0.935	0.8832	0.8313
ΔN_s	MW	0.3905	0.608	0.8959	1.1604	1.3513

The main result, apart from the thermodynamic parameters, is the number of axial stages, respectively: 27 stages for the high-pressure part (GT) and 6 stages for the low-pressure part (GT^{bap}) as shown in Fig.2. The length of the rotor blade of the last stage reached l_w =1.57 m and this is a value comparable

to the blades that operate in the newest steam unit in Kozienice Power Plant. In addition, it should be mentioned that this turbine is double-housed: high pressure (GT) and low-pressure (GT^{bap}) parts, and that the low-pressure part has double outlet.

3.2 CFD model in 3D simulation

Steady-state Reynolds Averaged Navier-Stokes (RANS) calculations were performed with the help of the commercial code Ansys CFX using second order spatial discretization with an automatic time step. The turbulence model used was k-ω SST of Menter [17]. The imposed set of boundary conditions consists of total pressure, total temperature and flow direction at the inlet, average static pressure at the outlet and rotational speed of the rotor domain. The frozen rotor technique is assumed to tackle the interface between the stationary and rotating domains. The rotor blades are unshrouded. The working fluid was described using through the NIST Refprop Thermodynamic and Transport properties database [18]. This models ale resolving set of basic equations, namely mass, momentum and energy balance equations for the fluid and energy dissipation equations. This set of basic equations can be written in the following manner:

- balance of mass - ρ:

$$\partial_t(\rho) + \mathrm{div}(\rho\mathbf{v}) = 0 \tag{5}$$

- balance of momentum - $\rho\mathbf{v}$:

$$\partial_t(\rho\mathbf{v}) + \mathrm{div}(\rho\mathbf{v} \otimes \mathbf{v} + p\mathbf{I}) = \mathrm{div}(\boldsymbol{\tau}^c) + \rho\mathbf{b} \tag{6}$$

- balance of energy - e:

$$\partial_t(\rho e) + \mathrm{div}(\rho e\mathbf{v} + p\mathbf{v}) = \mathrm{div}\left(\boldsymbol{\tau}^c\mathbf{v} + \mathbf{q}^C_{fluid}\right) + \rho\mathbf{b} \cdot \mathbf{v} \tag{7}$$

where: $\rho = \rho(\mathbf{x}, t)$ - fluid density, generally dependent on time t and location $\mathbf{x}$, $\mathbf{v} = v_i\boldsymbol{e}_i$ - fluid velocity, p - thermodynamical pressure, $\mathbf{I} = \delta_{ij}\boldsymbol{e}_i \otimes \boldsymbol{e}_j$ - unity tensor, $\boldsymbol{\tau}^c = \boldsymbol{\tau} + \boldsymbol{R} + \boldsymbol{D}$ - the viscous, turbulent and diffusive flux of momentum, $\mathbf{b}$ - mass force of Earth gravity, $e = u + \frac{\mathbf{v}^2}{2}$ - sum of internal and kinetic energy, $\mathbf{q}^C_{fluid} = \mathbf{q} + \mathbf{q}^+ + \mathbf{q}^{ph} + \ldots$ - total heat flux in the fluid. In order to take into account the influence of turbulent transport of momentum and turbulent transport of heat the fluid should possess the set of additional equations governing the evolution of turbulent primary parameters, for instance turbulent kinetic energy k and turbulent dissipation energy ω [19,20]:

$$\partial_t(\rho k) + \mathrm{div}(\rho k\mathbf{v}) = \mathrm{div}(\mathbf{J}_k) + \mathrm{S}_k \tag{8}$$

$$\partial_t(\rho\omega) + \mathrm{div}(\rho\omega\mathbf{v}) = \mathrm{div}(\mathbf{J}_\omega) + \mathrm{S}_\omega \tag{9}$$

where: - $\mathbf{J}_k$, $\mathbf{J}_\omega$ - diffusive flux of k and diffusive flux of ω with sources S_k, S_ω (various definitions of different authors exist in literature). For each finite volume of the computational grid seven equations are solved (one for mass, energy, k and ω transport balance equation and three momentum balance equations). The five balance equation (that consist of one mass balance equation, three momentum balance equations and one energy balance equation) and two evolution equation for parameters defining turbulence (equation for turbulent kinetic energy evolution k and equation for turbulence dissipation evolution ω) have been described in publications [20,21]. The turbulent viscosity in (8) and (9) is computed by combining k and ω as follows [19-21]:

$$\mu_t = \alpha^* \frac{\rho k}{\omega} \tag{10}$$

For low fluid velocities (laminar-turbulent transitions) the coefficient α^* damps the turbulent viscosity causing a low Re number correction. It is given by [19-21]:

$$\alpha^* = \alpha_\infty^*\left(\frac{\alpha_0^* + Re_t/R_k}{1 + Re_t/R_k}\right) \tag{11}$$

where: α_0^* - 0,024, R_k - 6, $Re_t = \frac{\rho k}{\mu\omega}$. For full turbulent flows the coefficient $\alpha^*$is equal 1.

4 Results analysis

It is worth noting the large velocity changes along the pitch diameter. At the hub velocity triangle that represents low degree of reaction is clearly visible Fig.4. At the apex the most different velocity triangle Fig 6 can be observed.

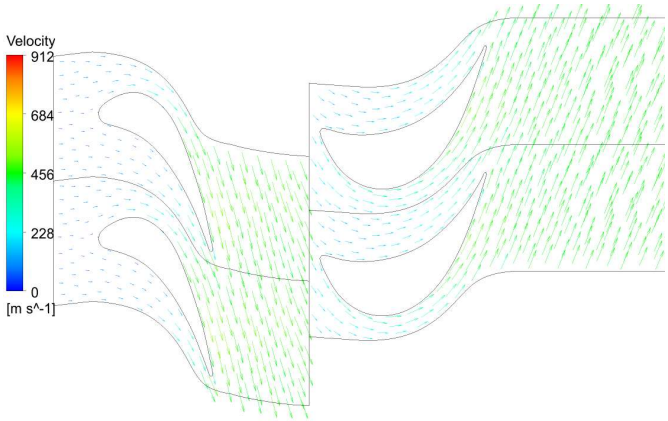

Figure 4: Velocity vectors at the hub.

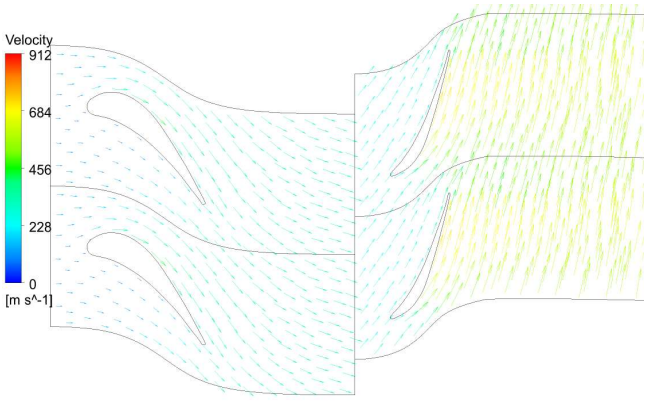

Figure 5: Velocity vectors at the mid-span.

In the Figure 4 we can see velocity vectors at the hub. This part of stage has low reaction ratio (0,1) and works like action stage. Most of expansion takes place at the rotor. Edge trail can be observed. Vortexes are not observed. Velocity vectors at the mid span are presented in the picture 5. This part of turbine has high reaction ratio (0,7), which is higher than in conventional impulse stage. Most expansion takes place at the rotor, what could be observed by values of velocity vectors. Vortexes does not appear. Flow conditions at the shroud are presented in the Figure 6. Reaction parameter is extremely high here (0,85). Radial change of shape of channel could be origin of vortex which could be observed. This part of stage should be redesigned with use of optimization algorithms.

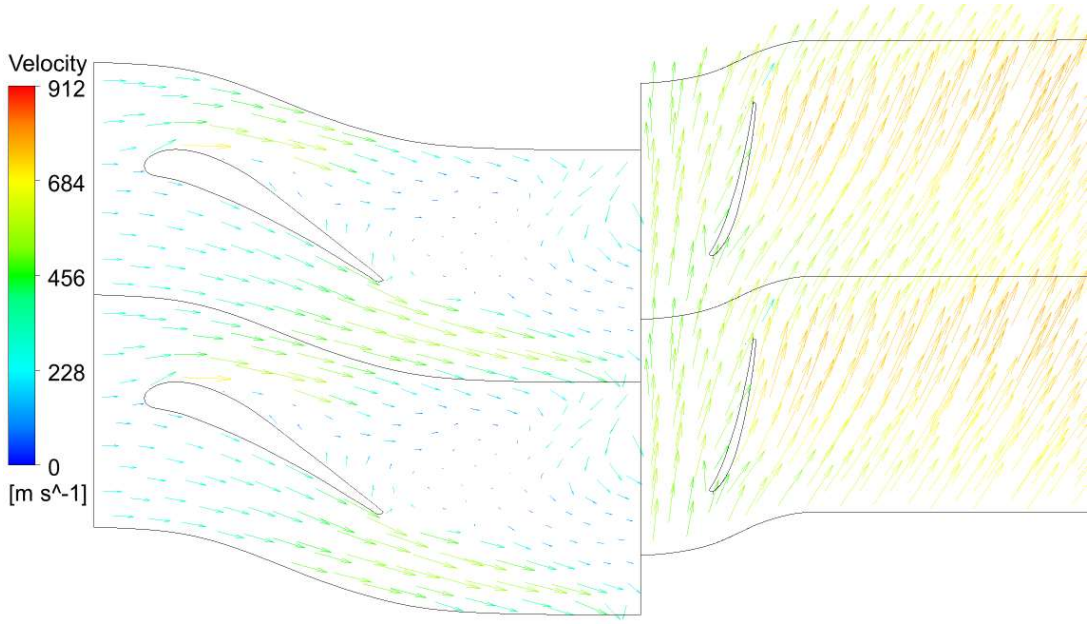

Figure 6: Velocity vectors at the shroud.

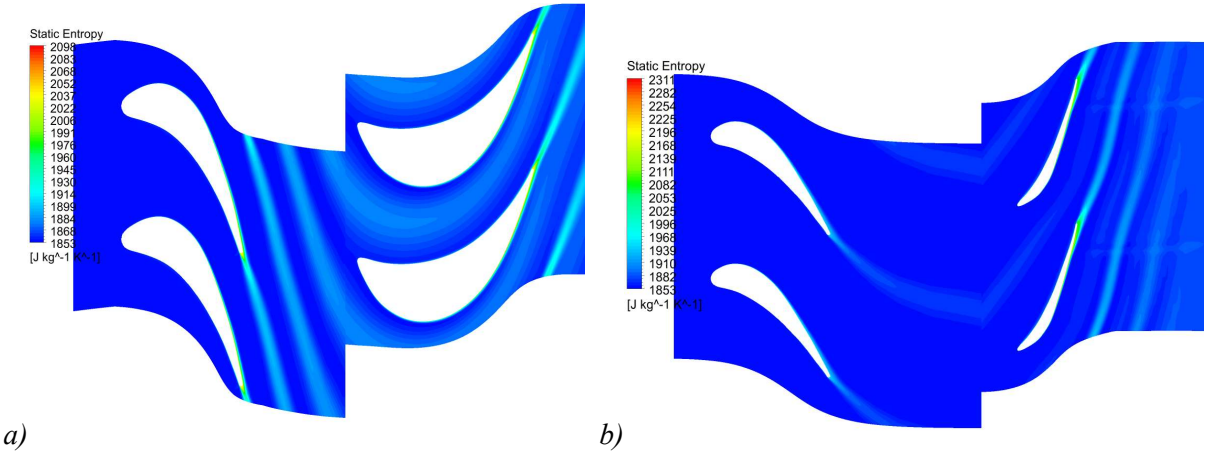

a) *b)*

Figure 7: Static entropy contours at the hub a) and Static entropy contours at the mid-span b).

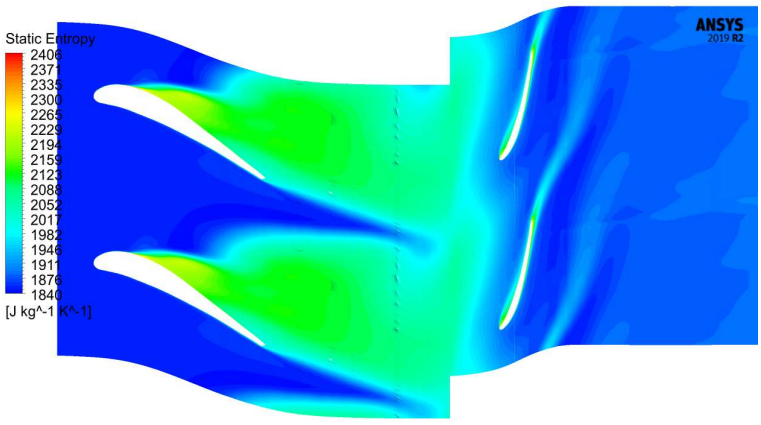

Figure 8: Static entropy contours at the shroud.

Static entropy contours shown in Fig. 7 - Fig. 8 indicate a high intensity of flow losses in shroud section of stator and rotor rows. In the mid-span and hub section the profile losses can be observed. Fig. 9 shows the distribution of loading through the rotor passage. The blade is more loaded closer to trailing edge of the blade. The pressure profiles in the hub is regular during whole axial distance. In the mid-span section occurs the higher pressure difference between suction and pressured side of the profile.

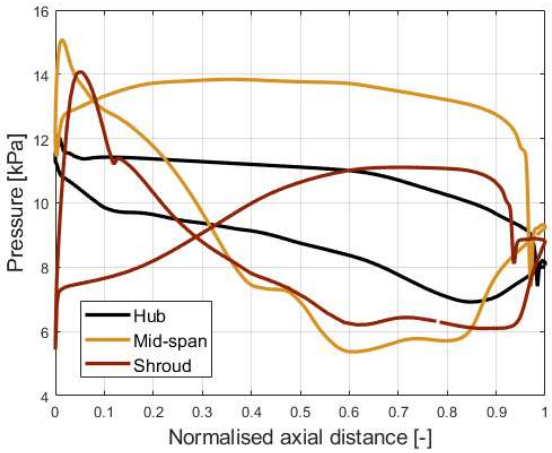

Figure 9: Rotor blade loading at the hub, mid-span and shroud.

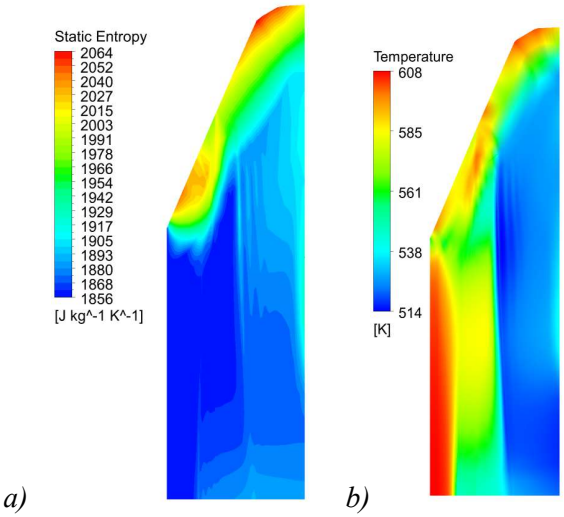

Figure 10: Static entropy contours in the stage a) and temperature b).

5 Conclusions

In this work the results obtained by the analytical method - free vortex - and the numerical method using CFD codes were compared. The analytical method allowed to determine the geometry of spatially twisted and trimmed vanes of the guide and rotor blades. Additionally, thermodynamic parameters, which were boundary conditions for CFD calculations, were determined using analytical methods. This information (geometry and thermodynamic parameters) was used as input data for CFD tool analysis. The velocity vectors and temperature fields showed a satisfactory agreement between the numerical and analytical calculations in the hub and mid-span (split radius) areas only. However, more attention should be focused on the essential differences that apply to the mass flow and the phenomena occurring at the top of the blade. The mass flow in analytical and in numerical terms reached 25 % differences. In addition, CFD calculations showed operation as ventilator in the upper edge area of both rotor and stator blades, resulting in temperature rise and significant entropy generation in this area. On the basis of the analysis, it should be concluded that the current shape of the channel should be redesigned in order to achieve the assumed mass flows of the working medium while maintaining the assumed efficiency.

References

[1] Szewalski R.: O racjonalne obliczanie długości łopatek w akcyjnych turbinach parowych. Czasopismo Techniczne, Vol 1, 1930, pp. 83-86.

[2] Szewalski R.: A novel design of turbine blading of extreme length. Trans IFFM, No 70-72, 1976, pp.137-143.

[3] Szewalski R.: Aktualne problemy rozwoju techniki energetycznej. Podwyższanie mocy jednostkowej i sprawności turbin oraz bloków energetycznych. Zakład Narodowy im. Ossolińskich. Wydawnictwo Polskiej Akademii Nauk, Wrocław-Warszawa-Kraków-Gdańsk(1978)

[4] Gardzilewicz A., Świrydczuk J., Badur J., Karcz M., Werner R., Szyrejko C.: Methodology of CFD computations applied for analyzing flows through steam turbine exhaust hoods. Trans. IFFM. Vol. 113, 2003, pp. 157–168.

[5] Knitter D., Badur J.: Sprzężona analiza 0D i 3D siły osiowej stopnia regulacyjnego turbiny parowej w zmiennych warunkach pracy. Systems, Vol. 13, 2008, pp. 244-262.

[6] Knitter D.: Zagadnienia adaptacji wlotu i wylotu turbiny parowej dla nowych warunków pracy. Rozprawa doktorska, IMP PAN, Gdańsk, Promotor J. Badur, (2008).

[7] Ziółkowski P.: Analiza termodynamiczna niskoemisyjnych obiegów gazowo-parowych z zastosowaniem oksyspalania. Rozprawa doktorska, IMP PAN, Gdańsk, Promotor J. Badur, (2018).

[8] Rubechini F., Marconcini M., Arnone A., Stefano C., Daccà F.:Some aspects of CFD modelling in the análisis of a low-pressure steam turbine. Proceedings of GT2007 ASME Turbo Expo 2007: Power for Land, Sea and Air

[9] Fiaschi D., Manfrida G., Maraschiello F.: Design and performance prediction of radial ORC turboexpanders, Applied Energy Vol. 138, 2015, pp. 517-532,

[10] Fiaschi d., Innocenti g.,, Manfrida G., Maraschiello F.:Design of micro radial turboexpanders for ORC power cycles: From 0D to 3D.Applied Thermal Engineering Vol 99, 2016,pp. 402-410,

[11] M.A. Noori Rahim Abadi, A. Ahmadpour, S.M.N.R. Abadi, J.P. Meyer.: CFD-based shape optimization of steam turbine blade cascade in transonic two phase flows. Applied Thermal Engineering, Vol. 112, 2017, pp. 1575-1589,

[12] Tanuma T., Okuda H., Hashimoto G., Yamamoto S., Shibukawa N., Okuno K., Saeki H., Tsukuda T.: Aerodynamic and Structural Numerical Investigation of Unsteady Flow Effects on Last Stage Blades. Proceedings of ASME Turbo Expo 2015: Turbine Technical Conference and Exposition GT2015.

[13] Tanuma T..: Development of last-stage long blades for steam turbines. Advances in Steam Turbines for Modern Power Plants. Woodhead Publishing, (2017), pp. 279-305.

[14] Touil K., Ghenaiet A.: Characterization of Vane - Blade Interactions in Two-stage Axial Turbine. Energy Vol. 172, Apr. 2019.

[15] Zhang, L. Y., He, L., Stuer, H.:A Numerical Investigation of Rotating Instability in Steam Turbine Last Stage. Proceedings of the ASME 2011 Turbo Expo: Turbine Technical Conference and Exposition.

[16] Perycz S.: Turbiny parowe i gazowe. Wyd. Pol. Gdańskiej, Gdańsk, (1988).

[17] Menter F. R., Kuntz M., Langtry R.: Ten Years of Industrial Experience with the SST Turbulence Model. Turbulence, Heat and Mass Transfer, Vol. 4, 2003, pp. 625–632.

[18] Lemmon E., Huber M., McLinden M.: REFPROP. National Institute of Standards and Technology. (2010).

[19] Wilcox D. C.: Turbulence Modeling for CFD. DCW Industries. Inc. La Canada, California, (1998).

[20] Kornet S., Ziółkowski P., Jóźwik P., Ziółkowski P.J., Stajnke M., Badur J.: Thermal-FSI modelling of flow and heat transfer in a heat exchanger based on minichannels. Journal of Power Technologies 97 (5) (2017) 373–381.

[21] Badur J., Charun H.: Selected problems of heat exchange modelling in pipe channels with ball turbulisers.: Archives of thermodynamics, Vol. 28 ,2007, pp. 65-87.